Electronic Supplementary Information

Interface Engineering in Crystalline/Amorphous Pd-Ru Heterostructures for Boosting Alkaline Hydrogen Oxidation Kinetics

Jianmei Wang,[a] Xiaozhong Zheng,[*b] Xinxin Shu,[c] Shun Li,[a] Jian Wu,[a] Cong Wang[a] and Lingzhi Kang[a]

[a]Institute of Ecology & Health, Hangzhou Polytechnic University, Hangzhou 310018, PR China.

[b]Department of Chemistry and Materials Science, Nanjing Forestry University, Nanjing 210037, China.

[c]School of Materials Science and Engineering, Zhejiang University, Hangzhou 310058, China.

Corresponding email: chemzxz@njfu.edu.cn

Experimental Section

Materials: All the chemicals were used as received without further purification. Ruthenium acetylacetonate ($Ru(acac)_3$), Potassium tetrachloropalladate(II) (K_2PdCl_4, purity 99.99%) and Nafion solution (5 wt%) were purchased from Alfa Aesar China Co. Ltd. Potassium bromide (KBr), ethylene glycol (EG, ≥99%), and ethanol (99.9%) were purchased from Sinopharm Chemical Reagent Co. Ltd. Potassium hydroxide (KOH, 90%) was purchased from Macklin. Carbon black (VulcanXC-72, purity 99.5%) was purchased from Alfa Aesar. Ultrapure deionized water (DIW) (18 MΩ cm^{-1}) was used in all the experiments.

Synthesis of Ru Nanosheets

Ru NS were synthesized using a modified method based on the previous work. In a typical procedure, 24 mg $Ru(acac)_3$ and 45 mg KBr were dissolved into a mixture solution containing 18 mL ethanol and 3 mL DIW. The resulting solution was stirred magnetically in a water bath at 50 °C until a dull red powder formed. The obtained powder was then calcined in a tube furnace at 280 °C for 1.5 h with a heating rate of 5 °C min^{-1} under an air atmosphere, followed by natural cooling to room temperature. The final product was washed several times with DIW and ethanol, collected by centrifugation, and freeze-dried.

Synthesis of Pd cluster/Ru NS

A series of Pd cluster/Ru NS samples with different Pd/Ru ratios were synthesized using a polyol reduction method. Typically, 5 mg of Ru NS and 38 mg of K_2PdCl_4 were dispersed in 20 mL of EG and sonicated for 2 min. The resulting suspension was then stirred vigorously (600 rpm) at 80 °C for 3 h to obtain $Pd_{4\%}$ cluster/Ru NS. The product was washed several times with DIW and ethanol, collected by centrifugation, and finally freeze-dried. $Pd_{2\%}$ cluster/Ru NS and $Pd_{10\%}$ cluster/Ru NS were prepared following the same procedure, using 15 mg and 100 mg of K_2PdCl_4, respectively. Here, $Pd_{2\%}$ cluster/Ru NS, $Pd_{4\%}$ cluster/Ru NS and $Pd_{10\%}$ cluster/Ru NS correspond to nominal Pd/Ru mass ratios of approximately 2%, 4%, and 10%,

respectively. Unless otherwise stated, "Pd cluster/Ru NS" in this work refers to $Pd_{4\%}$ cluster/Ru NS.

Synthesis of Pd/CB

Pd/CB was also prepared via the polyol reduction method. In a typical procedure, 5 mg of carbon black (CB) and 50 mg of K_2PdCl_4 were dispersed in 20 mL of EG and sonicated for 10 min. The mixture was then stirred vigorously (600 rpm) at 80 °C for 3 h to yield Pd/CB.

Material characterizations

X-ray diffraction (XRD) analysis was performed on a Rigaku Dmax-rc diffractometer using Ni-filtered Cu Kα radiation (λ = 1.5418 Å). Transmission electron microscopy (TEM) and high-resolution transmission electron microscopy (HRTEM) images were acquired using an FEI Tecnai G2 F20 S-TWIN microscope operated at 200 kV to investigate the morphology and microstructure of the samples. X-ray photoelectron spectroscopy (XPS) measurements were conducted on a VG Scientific ESCALab220i-XL spectrometer with monochromatic Al Kα radiation (500 μm spot size). The base pressure in the analysis chamber was maintained at approximately 3×10^{-10} mbar. Inductively coupled plasma mass spectrometry (ICP-MS) was carried out on an ICAP-RQ instrument (ThermoFisher Scientific, Germany) to determine the elemental compositions of the samples.

Electrochemical measurements

Electrochemical assessments were performed using a CHI 760E electrochemical workstation in a standard three-electrode cell. A glassy carbon electrode (GCE, 5 mm diameter) coated with the catalyst served as the working electrode, while a graphite rod and a Hg/HgO electrode were used as the counter and reference electrodes, respectively. The catalyst ink was prepared by dispersing a specific amount of catalysts in a 0.5 mL solution of isopropanol/H_2O (3/1) containing 5 μL of 5% Nafion solution. Subsequently, 10 μL of the electrocatalyst ink was applied to the GCE surface to maintain a low noble metal loading of 10 μg cm^{-2}. HOR assessments were performed in H_2-saturated 0.1 M KOH solution. The tests were conducted at

a scanning rate of 2 mV s^{-1} with a rotating speed of 1600 rpm, unless specific noted.

The kinetic current (j_K) was calculated based on the Koutecky–Levich equation:

$1/j=1/j_K+1/j_D$ (1)

where j stands for the measured current and j_D represents the diffusion current.

The specific exchange current density (j_o) was obtained by fitting j_K with Butler-Volmer equation:

$j_K=j_o[exp(\alpha F\eta/RT) - exp[-(1-\alpha)F\eta/RT]]$ (2)

where α is the charge transfer coefficient, R is the universal gas constant (8.314 J mol^{-1} K^{-1}), and T is the temperature (K), α and j_o were set as variables.

ECSA tests

Cu underpotential deposition (Cu-UPD) measurements were conducted to determine the electrochemically active surface area (ECSA). The Pd/C and Ru-based electrodes were polarized at the Cu-UPD potential for 100 s in an Ar-purged 0.5 M H_2SO_4 solution containing 5 mM $CuCl_2$ to achieve monolayer Cu deposition. Subsequently, Cu-UPD stripping voltammetry was carried out in $CuCl_2$-free 0.5 M H_2SO_4 at a scan rate of 10 mV s^{-1}. The voltammogram collected in $CuCl_2$-free electrolyte without Cu deposition was used as the background. The ECSA was evaluated from the integral area of Cu-UPD peaks (Q_{Cu}) with the subtraction of the background and a charge density of 420 μC cm^{-2} (Q_s):

ECSA (m^2_{metal}/g_{metal})= $Q_{Cu}/(M_{metal}*Q_s)$

where M_{metal} is the metal mass loading on a certain geometric area of the working electrode.

Computational details for calculations

Density functional theory (DFT) calculations in this study were conducted using Vienna ab-initio simulation package (VASP) with the Perdew-Burke-Ernzerhof (PBE) function for potential exchange-correlation.The projector augmented wave pseudopotentials method was employed to describe electron-ion interactions. A cut-off energy of 400 eV was used. The Gaussian smearing with a width of 0.05 eV was adopted around the Fermi surface. A vacuum

of 15 Å was included along the z-axis. Electronic structure calculations employed a (5 × 5 × 1) Monkhoest–Pack k-point mesh, while structure optimization used a (2 × 2 × 1) mesh. Geometry optimization was initiated when the forces reached a convergence criterion of less than 0.02 eV $Å^{-1}$, and the energy difference was below 10^{-4} eV. For Pd cluster/Ru NS and Pd/CB catalysts, the slab model was constructed by 8 Pd atoms supported on amorphous Ru substrate or monolayer graphene. During slab calculations, all atoms were allowed to relax. To obtain the thermodynamically stable amorphous Ru configuration, a constant-size NVT ensemble was utilized for AIMD (ab initio molecular dynamics) with an analog anneal-to-quench procedure starting at 1273.15 down to 298.15 K with total 45 Ru atoms. The total simulation time was 5 ps with a time step of 1 fs, and 5 000 steps were done to acquire the amorphous structure. When the simulation ended, additional geometry optimizations were carried out to obtain the stabilized amorphous structure.

The d-band center value (E_d) was determined by using $E_d = \int_{-\infty}^{\infty} N_d(\varepsilon)\varepsilon d\varepsilon \Big/ \int_{-\infty}^{\infty} N_d(\varepsilon) d\varepsilon$, where ε is the energy referring to Fermi level and $N_d(\varepsilon)$ is density of states (DOS) projected onto d-states or different orbits of d-states.

The charge accumulation and depletion were obtained as $\rho_{difference} = \rho_{Pd/Ru} - (\rho_{Pd} + \rho_{Ru})$, where ρ represents the charge density. The adsorption energy (E_{ads}) of OH* and H* is calculated by $E_{ads} = E(X/slab) - E(X) - E(slab)$, where X is adsorbate and slab is the model. The thermodynamic free energies (G) were calculated using the equation $G = E_{DFT} + E_{ZPE} - TS$, where E_{DFT} represents the DFT ground state, E_{ZPE} stands for zero-point energy, and S corresponds to entropy.

Figures and Tables

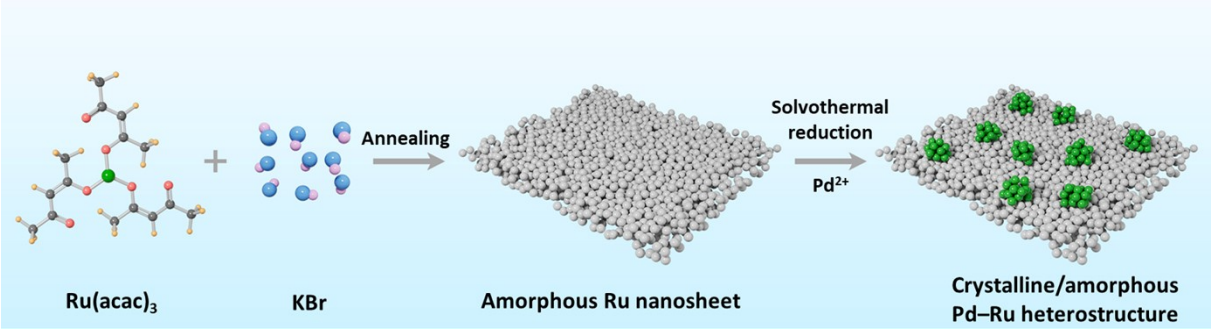

Fig. S1. Schematic illustration of the synthetic process for Pd cluster/Ru NS.

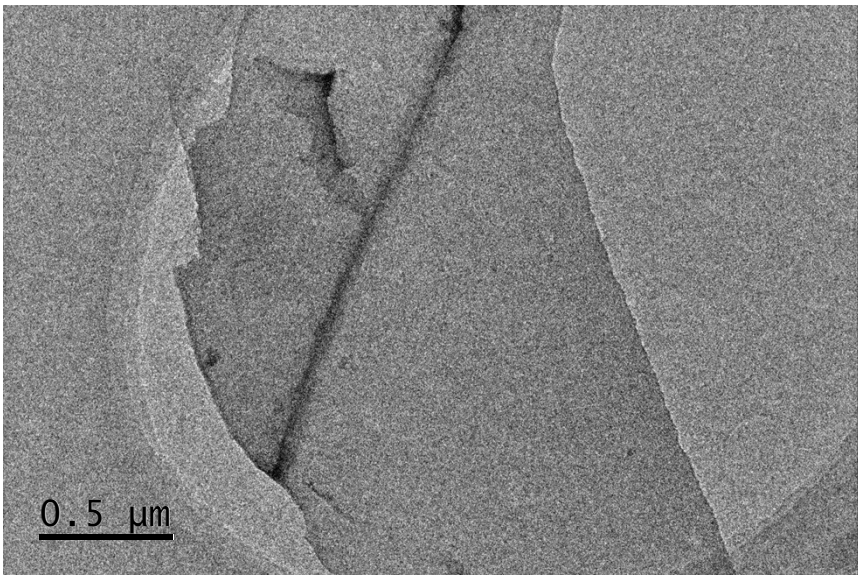

Fig. S2. TEM image of Ru NS.

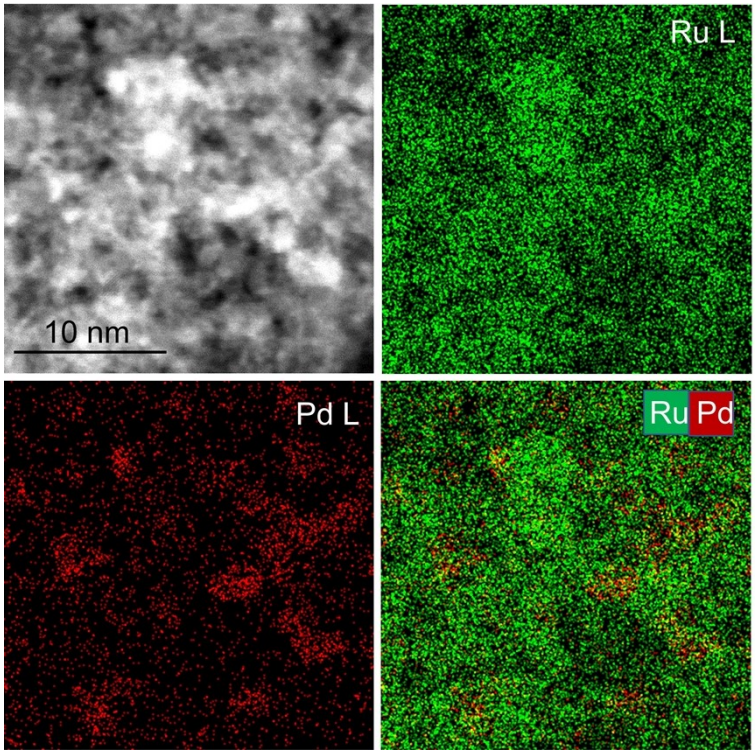

Fig. S3. EDS element mapping images of Pd cluster/Ru NS.

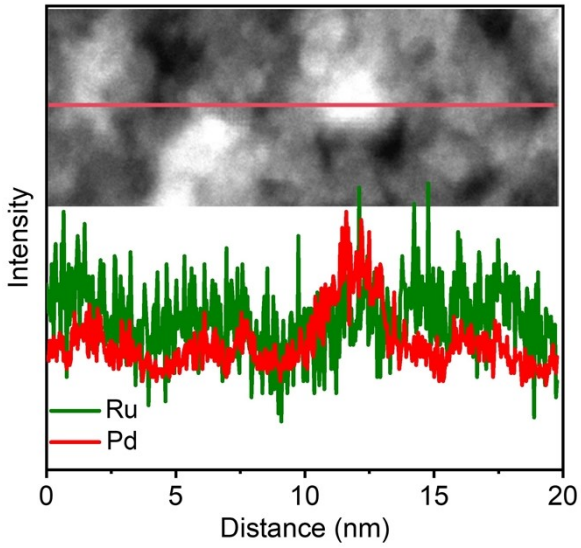

Fig. S4. EDS line-scanning profiles across the Pd cluster/Ru NS.

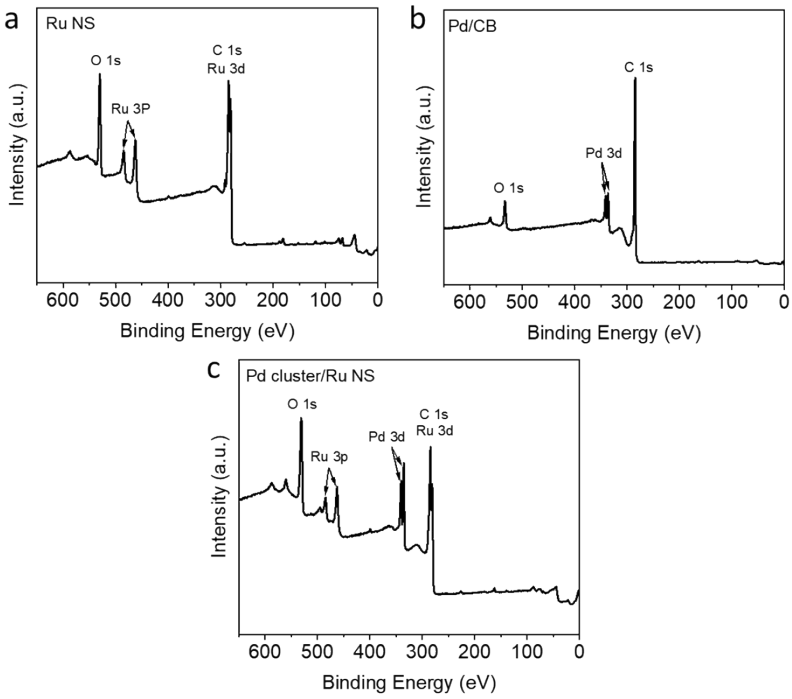

Fig. S5. XPS survey spectra of (a) Ru NS, (b) Pd/CB and (c) Pd cluster/Ru NS samples.

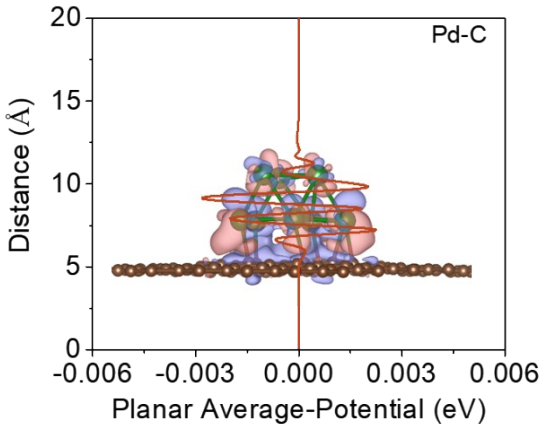

Fig. S6. Planar average potential of Pd_8/C model along the *Z*-direction. The insert is charge density difference, where the red region reflects an electron-deficient state while the bright blue region reflects an electron-rich area, with an isovalue of 0.005 $e^-/Å^3$.

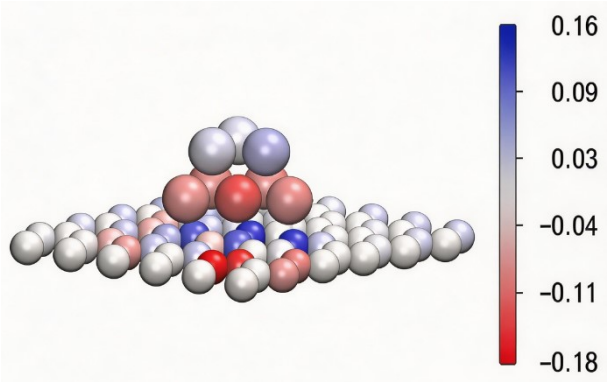

Fig. S7. The bader charge distribution of Pd_8/C model.

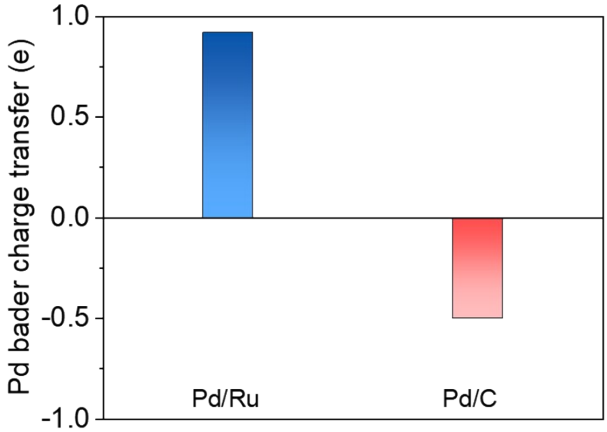

Fig. S8. Pd bader charge transfer in Pd_8/Ru and Pd_8/C.

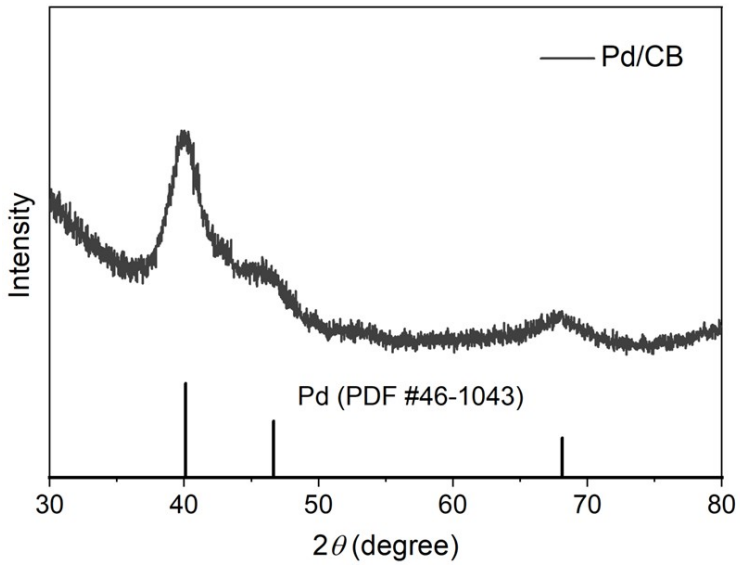

Fig. S9. XRD spectra of Pd/CB.

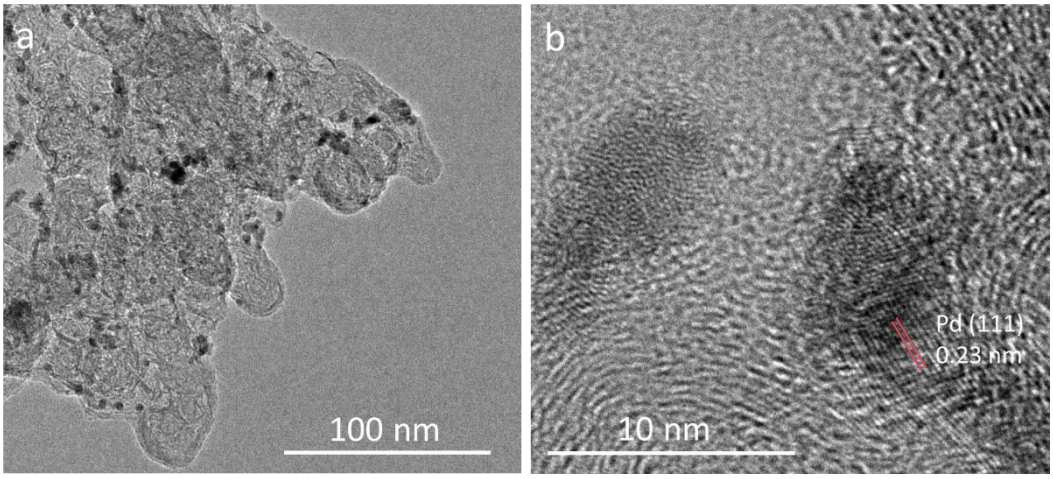

Fig. S10. (a) TEM image of Pd/CB. (b) HRTEM image of Pd/CB.

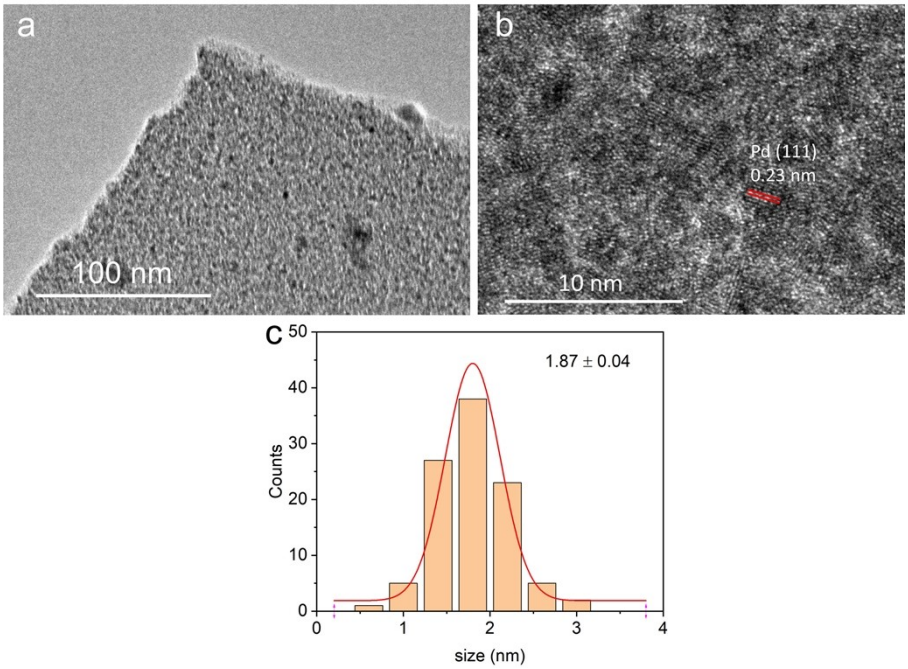

Fig. S11. TEM (a) and HRTEM (b) images of $Pd_{2\%}$ cluster/Ru NS. (c) The size distribution histogram of the Pd clusters in the $Pd_{2\%}$ cluster/Ru NS samples.

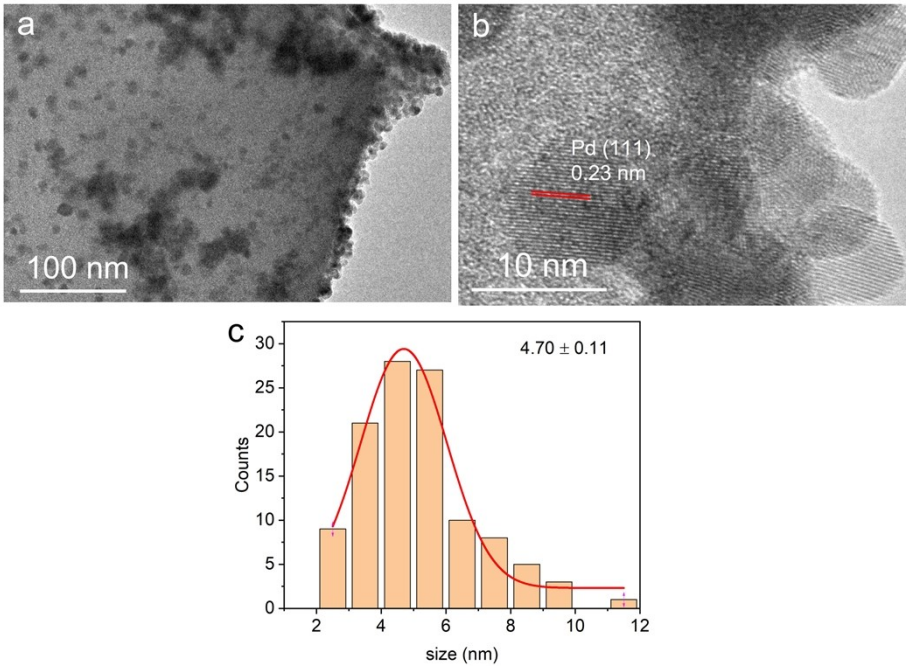

Fig. S12. TEM (a) and HRTEM (b) images of $Pd_{10\%}$ cluster/Ru NS. (c) The size distribution histogram of the Pd clusters in the $Pd_{10\%}$ cluster/Ru NS samples.

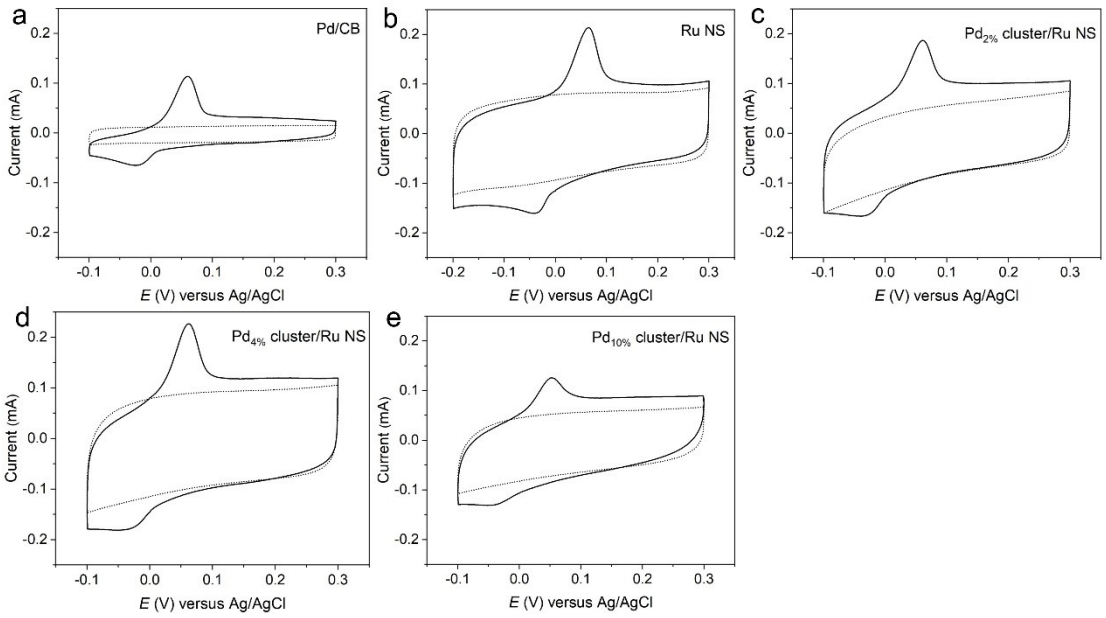

Fig. S13. Estimation of the ECSA using the copper underpotential deposition (Cu-UPD) method for Pd/CB (a), Ru NS (b), $Pd_{2\%}$ cluster/Ru NS (c), $Pd_{4\%}$ cluster/Ru NS (d) and $Pd_{10\%}$ cluster/Ru NS (e).

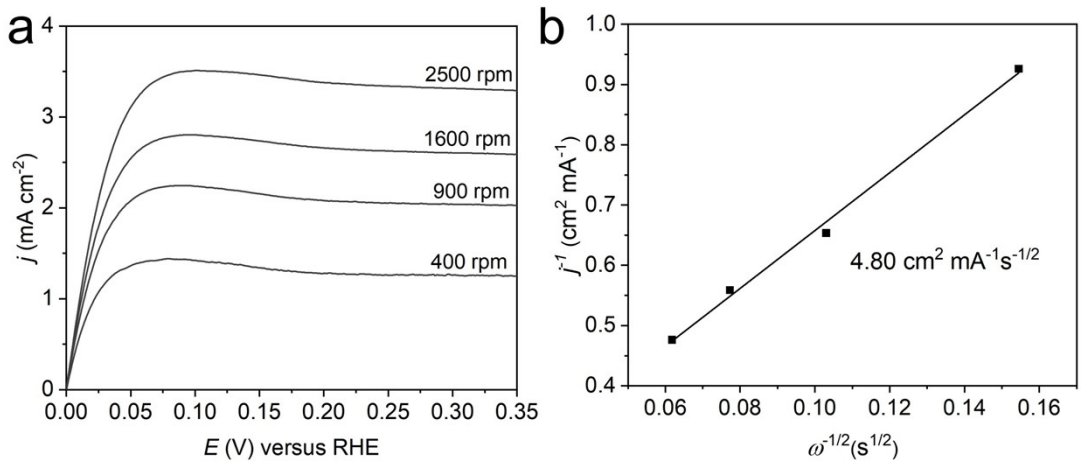

Fig. S14. (a) HOR polarization curves of Pd cluster/Ru NS sample at different rotation speeds. (b) The Koutecky-Levich plot of Pd cluster/Ru NS at an overpotential of 25 mV derived from Fig. S14a.

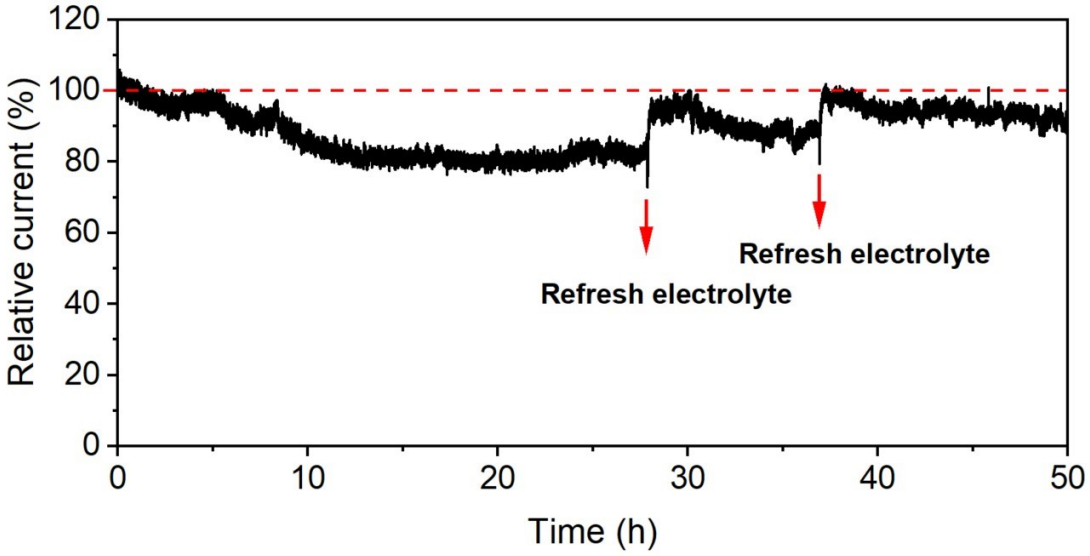

Fig. S15. Relative current–time chronoamperometric response of the Pd cluster/Ru NS catalyst supported on carbon fiber paper with a precious metal loading of 100 μg cm^{-2} at an overpotential of 100 mV in 0.1 M KOH solution.

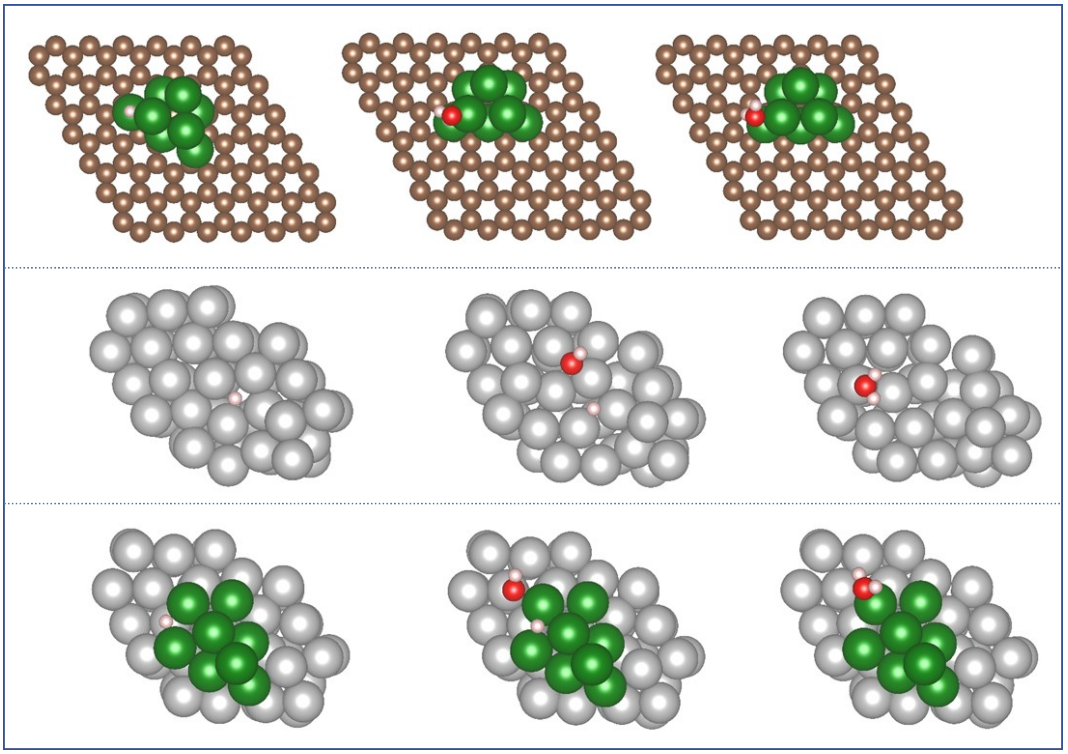

Fig. S16. TOP view of the atomic configurations of different models.

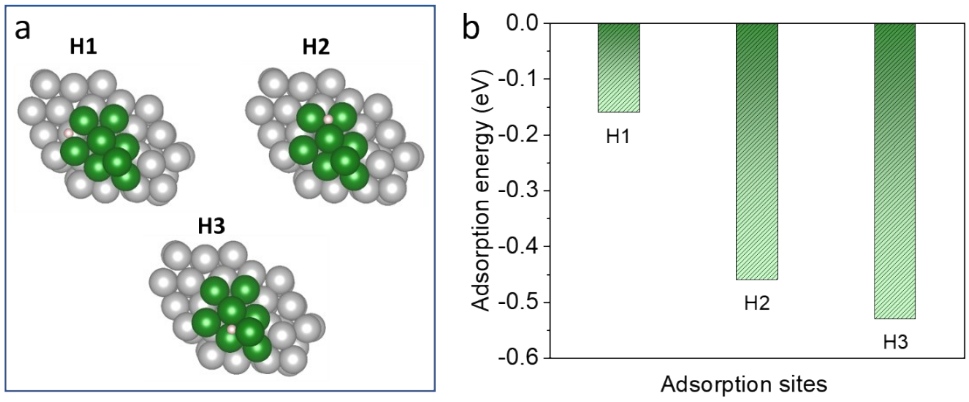

Fig. S17. (a) Different adsorption sites of H* on the model of Pd/Ru. (b) Adsorption energy of H* on different adsorption sites illustrated in (a).

Table S1. Chemical compositions of different sample catalysts determined by ICP-OES.

Sample	Pd (wt%)	Ru (wt%)
Ru NS	-	68.47
Pd/CB	5.74	-
$Pd_{2\%}$ cluster/Ru NS	1.35	68.31
$Pd_{4\%}$ cluster/Ru NS	2.79	67.12
$Pd_{10\%}$ cluster/Ru NS	6.23	63.59

Table S2. Alkaline HOR performance comparison of the electrocatalysts applied in this study.

Catalyst	ECSA ($m^2\ g^{-1}$)	Loading ($\mu g\ cm^{-2}$)	j_k@30 mV (mA cm_{ECSA}^{-2})	j_o(mA cm_{GEO}^{-2})	j_o(mA cm_{ECSA}^{-2})	j_o(A mg_{PGM}^{-1})
Ru NS	92.8	10	0.352	2.25	0.243	1.15
Pd/CB	55.4	10	0.009	0.05	0.009	0.03
$Pd_{2\%}$ cluster /Ru NS	61.7	10	0.435	2.74	0.444	1.40
$Pd_{4\%}$ cluster /Ru NS	73.7	10	0.982	5.47	0.744	2.79
$Pd_{10\%}$ cluster /Ru NS	40.1	10	0.579	1.76	0.438	0.90

Table S3. Comparison of HOR activity with previous reported Ru-based catalysts in 0.1 M KOH.

Electrode modification	j_o (mA cm^{-2})	$j_{k,m}$@50 mV（A mg_{PGM}^{-1}）	Ref.
Ru colloidosomes	2.86	/	1
$Co_1Ru_{1,n}$/rGO	0.68	7.68	2
RuNi/NC	2.69	/	3
$Mn_1O_x(OH)_y$@Ru/C	2.05	/	4
Ru@C	3.48	/	5
Ru-Ru_2P/C	/	1.265	6
Ru-B-C–350	/	0.88	7
Ruc/NHCS	1.74	1.95	8
Ru-TiO_2-450	5.92	1.529	9
Ru NAs with fcc phase	8.16	2.75	10
Pd cluster/Ru NS	5.47	2.76	This work

$Co_1Ru_{1,n}$/rGO: symmetry structure of Ru nanoparticles by embedding cobalt (Co) single atoms on reduced graphene oxide;
RuNi/NC: Ru-Ni diatomic sites supported on N-doped porous carbon;
$Mn_1O_x(OH)_y$@Ru/C: $Mn_1O_x(OH)_y$ clusters-modified Ru nanoparticles;
Ru@C: defective-carbon-supported Ru catalyst;
Ru–B–C–350:Borophene–Confined Ru Clusters;
Ruc/NHCS:Ru clusters supported on nitrogen-doped hollow carbon spheres;
Ru NAs:Ru nanosheet assemblies.

References

1 X. Yang, B. Ouyang, P. Shen, Y. Sun, Y. Yang, Y. Gao, E. Kan, C. Li, K. Xu and Y. Xie, *J. Am. Chem. Soc.*, 2022, **144**, 11138–11147.

2 X. Q. Mu, S. L. Liu, M. Y. Zhang, Z. C. Zhuang, D. Chen, Y. R. Liao, H. Y. Zhao, S. C. Mu, D. S. Wang and Z. H. Dai, *Angew. Chem. Int. Ed.*, 2024, **63**, e202319618.

3 L. Han, P. Ou, W. Liu, X. Wang, H. T. Wang, R. Zhang, C. W. Pao, X. Liu, W. F. Pong, J. Song, Z. Zhuang, M. V. Mirkin, J. Luo and H. L. Xin, *Sci. Adv.*, 2022, **8**, eabm3779.

4 H. Shi, Y. Yang, P. Meng, J. Yang, W. Zheng, P. Wang, Y. Zhang, X. Chen, Z. Cheng, C. Zong, D. Wang and Q. Chen, *J. Am. Chem. Soc.*, 2024, **146**, 16619–16629.

5 Z. Yang, W. Lai, B. He, J. Wang, F. Yu, Q. Liu, M. Liu, S. Zhang, W. Ding, Z. Lin and H. Huang, *Adv. Energy Mater.*, 2023, **13**, 2300881.

6 L. Su, Y. Jin, D. Gong, X. Ge, W. Zhang, X. Fan and W. Luo, *Angew. Chem. Int. Ed.*, 2023, **62**, e202215585.

7 M. Wang, J. Liu, N. Sun, L. Wang, Z. Lou, X. Cui and L. Jiang, *Adv. Funct. Mater.*, 2026, **36**, e14712.

8 G. Meng, H. Cao, T. Wei, Q. Liu, J. Fu, S. Zhang, J. Luo and X. Liu, *Chem. Commun.*, 2022, **58**, 11839-11842.

9 X. Jin, X. Zhang, B. Yang, X. Zheng, M. Gao, H. Pan and W. Sun, *J. Mater. Chem. A*, 2025, **13**, 20404-20411.

10 J. Zhang, M. Cao, X. Li, Y. Xu, W. Zhao, L. Chen, Y. C. Chang, C. W. Pao, Z. Hu and X. Huang, *Small*, 2023, **19**, 2207038.